Structural and optical properties of paraelectric $SrTiO_3$

2000 J. Phys.: Condens. Matter 12 3325

(http://iopscience.iop.org/0953-8984/12/14/309)

J. Phys.: Condens. Matter **12** (2000) 3325–3336. Printed in the UK PII: S0953-8984(00)10902-6

Structural and optical properties of paraelectric $SrTiO_3$

Sonali Saha†, T P Sinha† and Abhijit Mookerjee‡

† Department of Physics, Bose Institute, 93/1, Acharya Prafulla Chandra Road, Calcutta-700009, India

‡ S N Bose National Centre for Basic Sciences, JD Block, Sector 3, Salt Lake City, Calcutta-700091, India

Received 12 January 2000

Abstract. The electronic energy band structure, site- and angular-momentum-decomposed densities of states (DOS) and charge-density contours of perovskite $SrTiO_3$ in the paraelectric cubic phase are calculated by the first-principles tight-binding linear muffin-tin orbitals method with atomic sphere approximation using density functional theory in its local density approximation. The calculated band structure shows a direct band gap of ∼1.4 eV at the gamma point in the Brillouin zone. The total DOS is compared with experimental x-ray photoemission spectra. From the DOS analysis, as well as charge-density studies, we conclude that the bonding between Sr and TiO_3 is mainly ionic and that the TiO_3 entities bond covalently. Using the projected DOS and band structure we have analysed the interband contribution to the optical properties of $SrTiO_3$. The real and imaginary parts of the dielectric function and hence the optical constants (such as the reflectivity, refractive index, extinction coefficient and absorption coefficient) and the electron energy-loss spectrum are calculated. The calculated spectra are compared with the experimental results for $SrTiO_3$ in the cubic phase and are found to be in good agreement with the experimental results in low-energy regions. The role of band-structure calculation as regards the optical properties of $SrTiO_3$ is discussed.

1. Introduction

Ferroelectric and related materials having the chemical formula ABO_3 have been the subjects of extensive investigation, both because of their technical importance and because of the fundamental interest in the physics of their phase transitions [1]. Within this family of materials, one finds transitions to a wide variety of low-symmetry phases, ranging from non-polar antiferrodistortive (AFD) to polar ferroelectric and antiferroelectric transitions. The ideal structure is cubic perovskite, where the A and B cations are arranged on a simple cubic lattice and the O ions lie on the face centres nearest the (typically transition metal) B cations. Thus the B cations are at the centres of O octahedra, while the A cations lie at larger twelvefold-coordinated sites. This ideal structure displays a wide variety of structural instabilities in the various materials. These may involve rotations and distortions of the O octahedra as well as displacements of the cations from their ideal sites. The interplay of these instabilities accounts for the rich variety of ferroelectric and antiferroelectric behaviours.

$SrTiO_3$ in this class has been the subject of ongoing theoretical and experimental studies because of its unusual dielectric property which deviates from those of other ABO_3 perovskites. While it has the simple cubic perovskite structure at high temperature, $SrTiO_3$ goes through an AFD transition at 105 K to a tetragonal phase in which the oxygen octahedra have rotated by a small angle along the *c*-axis in opposite senses in neighbouring unit cells. The dielectric

0953-8984/00/143325+12$30.00

response follows a Curie–Weiss law at higher temperature, suggesting a ferroelectric phase transition at about 35–40 K. But the dielectric constant does not show a peak at atmospheric pressure at any finite temperature. It continues to rise down to helium temperature and finally attains a maximum value [1]. The suppression of the ferroelectric long-range ordering is due to quantum fluctuation which induces a quantum paraelectric phase at very low temperature [2]. The 105 K transition involves the instability of a zone-boundary mode [1]. Quantum fluctuation can only lower this transition temperature because of its 2D disc-like correlation which suppress its effect on the AFD [3]. In the tetragonal phase the unit-cell volume remains unchanged with the small tetragonal distortion $c/a = 1.0005$ [4].

Spitzer *et al* [5] have measured the infrared reflectivity spectra of $SrTiO_3$ at room temperature and from these data they have calculated the principal dielectric response functions using Kramers–Krönig relations. Perkins and Winter [6] have studied the electronic structure of $SrTiO_3$ related to the dielectric function using band-structure calculation by the LCAO method. Investigations have been carried out to study the structural [4], dielectric [7], optical [8,9] and elastic [10] properties, and the infrared [11,12] as well as electron paramagnetic resonance [13] spectra of $SrTiO_3$. A recent study using gamma-ray diffraction has indicated the origin of the quantum mechanical suppression where the zero-point motion of the Ti ions (0.053 Å) has larger magnitude than the zero-temperature ferroelectric displacement of Ti (0.043 Å) towards an off-centre position [14]. Although various properties [2–16] of $SrTiO_3$ have been investigated, a systematic theoretical study of the optical properties based upon first-principles band-structure calculations is still lacking.

In the present study, the electronic structure and optical properties of cubic perovskite $SrTiO_3$ in the paraelectric phase are calculated by the first-principles tight-binding linearized muffin-tin orbital (TB-LMTO) method with atomic sphere approximation (ASA) using density functional theory (DFT) in its local density approximation (LDA) [17]. The first-principles density functional calculations offer an attractive approach for enhancing our microscopic understanding of perovskites. The all-electron full-potential linearized augmented-plane-wave method has been used by several groups to study ferroelectricity in perovskites within the LDA [18–21]. Recently, King-Smith and Vanderbilt performed a systematic study of structural and dynamical properties and energy surfaces for eight common perovskites, using the first-principles ultrasoft-pseudopotential method and the LDA [22,23]. These calculations demonstrate that ferroelectricity in the perovskites reflects a delicate balance between long-range electrostatic forces which favour the ferroelectric state and short-range repulsions which favour the cubic phase. In the forthcoming sections, the computational details regarding the methods used in our calculations of the electronic structure and optical properties are described. Finally, the calculated results are compared with available experimental data [6,9].

2. Computational details

The paraelectric phase of $SrTiO_3$ has the ideal cubic $Pm3m$ perovskite structure, in which the oxygen octahedron contains a Ti atom at its centre. The cubic unit cell contains one molecule with the Sr sitting at the origin $(0.0, 0.0, 0.0)a$, the Ti at the body centre $(0.5, 0.5, 0.5)a$ and the three oxygen atoms at the three face centres $(0.5, 0.5, 0.0)a$, $(0.0, 0.5, 0.5)a$ and $(0.5, 0.0, 0.5)a$. The lattice constant is 7.38 au, taken from the experimental results of Wyckoff [24]. Figure 1(a) shows the unit cell and figure 1(b) the Brillouin zone of $SrTiO_3$ for this structure, whereas figure 1(c) shows the rotation of oxygen octahedra about one of the cubic axes passing through the Ti atom in opposite senses in all adjacent cells.

We present here electronic structure calculations made using the TB-LMTO. The calculations were done within the ASA. The basis sets used here comprised augmented linear

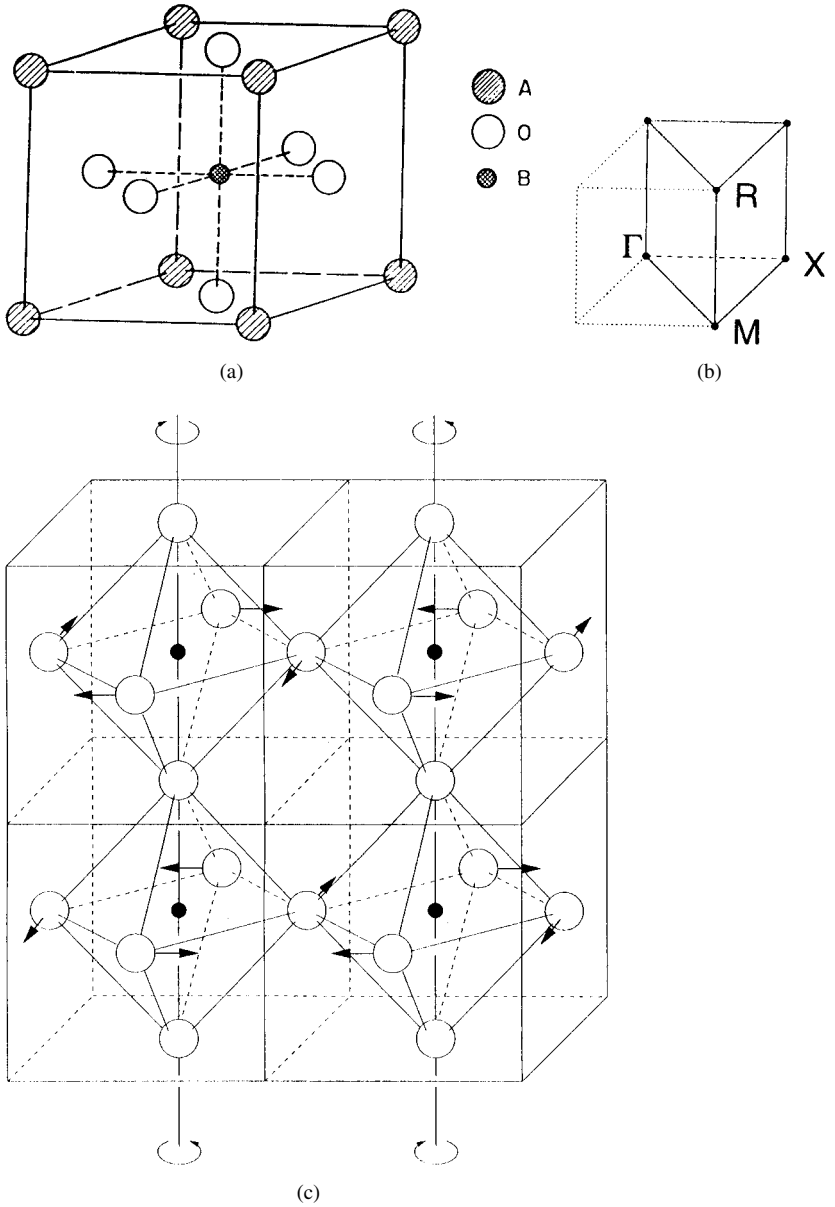

Figure 1. (a) The cubic unit cell of $SrTiO_3$. (b) The Brillouin zone for the cubic crystal. (c) The rotation of O octahedra about the *c*-axis in opposite senses in all adjacent cells.

muffin-tin orbitals. Within the atomic spheres, the basis functions, the charge density and the potential are expanded in symmetry-adapted, spherical harmonics together with a radial function. Basis functions up to $\ell_{max} = 3$ for Sr and $\ell_{max} = 2$ for Ti and O were used. The calculations were carried out within the LDA and the radial part of the basis was obtained by solving a Schrödinger-like Kohn–Sham equation in which the scalar relativistic corrections were incorporated. The von Barth–Hedin exchange potential was used. The volume ratio between the atomic spheres and the unit cells was 1, so no empty spheres were necessary.

The atomic sphere overlap was <15%. Brillouin-zone integration was carried out using the tetrahedron method using a mesh of about 200 symmetry-reduced points. The Sr 5p and the O 3s and 3d orbitals were downfolded and do not contribute to the dimension of the Hamiltonian (H) and the overlap (O) matrices, but carry charge. This downfolding avoided the appearance of ghost bands.

The linear response of the system to an external electromagnetic field with a small wave vector is measured through the complex dielectric function $\epsilon(\omega)$. The frequencies of interest to us will be well above those of phonons, so we shall consider the electronic excitations alone. This we shall do within the random-phase approximation. Local field and lifetime effects will be neglected. Lifetime broadening will be reintroduced subsequently phenomenologically by convoluting the absorptive part of $\epsilon(\omega)$ with a Lorentzian with a full width at half-maximum (FWHM) of 8×10^{-4} Ryd at the photon energy of 0.073 Ryd, increasing quadratically with photon energy, as suggested by Ravindran *et al* [25]). The cubic nature of $SrTiO_3$ leads to a diagonal and isotropic dielectric tensor. The imaginary part of the dielectric function $\epsilon''(\omega)$ is then given by

$$\epsilon''(\omega) = \left(\frac{Ve^2}{2\pi\hbar\, m^2\omega^2}\right) \int \mathrm{d}^3\boldsymbol{k} \sum_{nn'} |\langle \boldsymbol{k}n|\boldsymbol{p}|\boldsymbol{k}n'\rangle|^2 f(\boldsymbol{k}n)(1 - f(\boldsymbol{k}n')\, \delta(E_{\boldsymbol{k}n} - E_{\boldsymbol{k}n'} - \hbar\omega). \tag{1}$$

Here $\hbar\omega$ is the energy of the incident photon, $\boldsymbol{p}$ is the momentum operator $(\hbar/\mathrm{i})\,\partial/\partial x$, $|\boldsymbol{k}n\rangle$ is a crystal wavefunction and $f(\boldsymbol{k}n)$ is the Fermi function. The other symbols have their usual meanings. It is often easier to convert from the reciprocal-space $\boldsymbol{k}$ as the variable of integration to the energy E and from the band index n to the LMTO indices L, α, where $L = (\ell, m)$ are angular momenta and α labels the particular atom in the unit cell. The expression (1) then becomes

$$\epsilon''(\omega) = \frac{A}{\omega^2} \int \mathrm{d}E \sum_{LL',\alpha\alpha'} T_{LL'}^{\alpha\alpha'}(E,\omega) n_L^{\alpha}(E) n_{L'}^{\alpha'}(E+\hbar\omega) f(E)(1 - f(E')) \tag{2}$$

where A is a constant, $n_L(E)$ is the angular-momentum-projected density of states, $f(E)$ is the Fermi function and the transition matrix $T_{LL'}(E,\omega)$ is given by

$$T_{LL'}(E,\omega) = \left| \int \mathrm{d}^3 r\; \phi_L^*(E,\boldsymbol{r})\, \frac{\partial}{\partial x} \phi_{L'}(E+\hbar\omega,\boldsymbol{r}) \right|^2 .$$

The matrix element is evaluated over the atomic spheres. In addition to the lifetime broadening which is introduced at this stage, an additional Gaussian broadening due to instrumental resolution of FWHM 4×10^{-4} Ryd was also incorporated.

The real part of the dielectric function $\epsilon'(\omega)$ follows from the Kramers–Krönig relationship. All optical constants may now be derived from this. If we assume orientation of the crystal surface parallel to the optical axis, the reflectivity $R(\omega)$ follows directly from Fresnel's formula:

$$R(\omega) = \left| \frac{\sqrt{\epsilon(\omega)} - 1}{\sqrt{\epsilon(\omega)} + 1} \right|^2 .$$

Expressions for the absorption coefficient $I(\omega)$, extinction coefficient $k(\omega)$, energy-loss spectrum $L(\omega)$ and refractive index $n(\omega)$ now follow immediately:

$$\begin{aligned} I(\omega) &= \sqrt{2}\omega(\sqrt{\epsilon'(\omega)^2 + \epsilon''(\omega)^2} - \epsilon'(\omega))^{1/2} \\ k(\omega) &= I(\omega)/2\omega \\ L(\omega) &= \epsilon''(\omega)/(\epsilon'(\omega)^2 + \epsilon''(\omega)^2) \\ n(\omega) &= (1/\sqrt{2})(\sqrt{\epsilon'(\omega)^2 + \epsilon''(\omega)^2} + \epsilon'(\omega))^{1/2}. \end{aligned} \tag{3}$$

It is to be noted that for the interpretation of the optical spectra of systems, it does not seem realistic to give a single transition assignment to the peaks present in a crystal reflection spectrum since many transitions (direct to indirect) may be found in the band structure with an energy corresponding to the peak and since states away from the lines and point of symmetry could contribute to the reflectivity. Therefore, the symmetry-allowed transition energies lead to an incomplete description of the optical spectrum. We have generated theoretical curves using the customary approximation made to interpret the optical spectra from band-structure calculations, namely by considering the imaginary part $\epsilon''(\omega)$ of the optical dielectric constant ϵ as proportional to the joint density of states weighted by ω^{-2}. The theoretical results are compared with the observed experimental data.

3. Results and discussion

3.1. Band structure and density of states

Since the optical spectra are calculated from interband transitions, we first describe our calculated electronic structure. The calculated band structure for paraelectric $SrTiO_3$ in the high-symmetry directions in the Brillouin zone is shown in figure 2. In the figure we find a large dispersion of the bands. Nine valence bands are derived from O 2p orbitals. These are separated by a direct gap ∼1.4 eV (at the G point) from the transition metal d-derived conduction band. This gap is somewhat lower than the experimental band gap 3.3 eV for $SrTiO_3$. The origin of this discrepancy may be the local density approximation which underestimates the band gaps even for insulators. The nine valence bands at the G point are the three triply degenerate levels (Γ_{15}, Γ_{25} and Γ_{15}) separated by energies of 1.73 eV (Γ_{15}–Γ_{25}) and 1.09 eV (Γ_{25}–Γ_{15}).

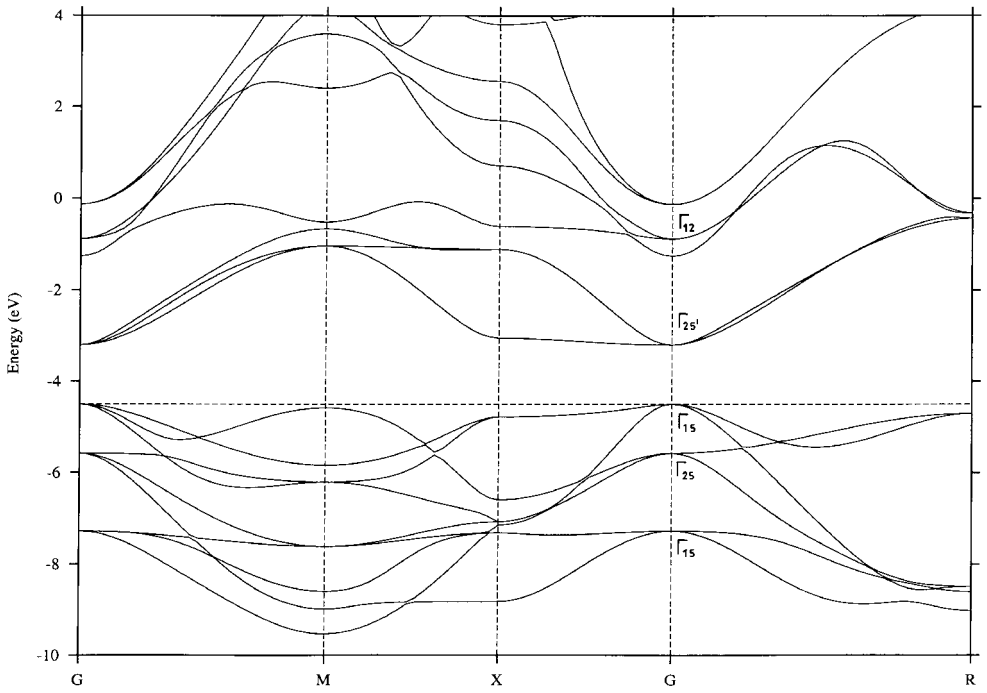

Figure 2. Calculated energy band structure of $SrTiO_3$.

These splittings are produced by the crystal field and the electrostatic interaction between O 2p orbitals. In the conduction band the triply ($\Gamma_{25'}$) and doubly (Γ_{12}) degenerate levels represent t_{2g} and e_g states of Ti 3d orbitals separated by an energy of 2.36 eV.

The calculated total DOS for $SrTiO_3$ in the valence band region along with experimental results (the x-ray photoemission spectroscopy (XPS) spectrum) [6] are shown in figure 3. The calculated DOS was convoluted with a Lorentzian of 0.5 eV full width at half-maximum. The Fermi level in the theoretical spectrum is set to zero on the energy scale. Our DOS exhibits sharper peaks than the experimental spectra, since we have not included the lifetime broadening in our DOS curve. The experimental bandwidth is 6.5 eV whereas our calculated result gives a band of width 5 eV. This reduction of bandwidth is due to the muffin-tin approximation. There is another discrepancy as regards the positions of peaks. In order to align the peaks, a rigid shift of 1 eV is needed for the calculated spectrum due to the previously mentioned underestimation of the band gap in the LDA formalism even for band insulators. To get more insight into the valence band spectra near the Fermi level, we show the angular-momentum- and site-decomposed DOS in figure 4. There exists a p–d hybridization as is evident from this figure. The Ti 3d contribution is zero at the valence band maximum but rises with increasing binding energy. Conversely the O 2p contribution rises from zero at the conduction band minimum with increasing energy. This reflects the Ti 3d–O 2p covalency.

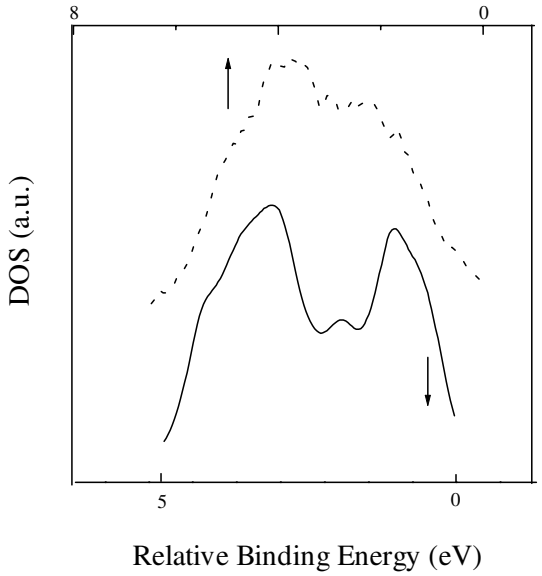

Figure 3. The calculated total DOS curve is compared with the XPS spectrum [6]: continuous line: theoretical; dashed line: experimental. The Fermi level in the theoretical spectrum is set to zero on the energy scale.

3.2. Chemical bonding

To have a clear picture of the nature of the chemical bonding between the constituents of $SrTiO_3$ in the paraelectric phase we have shown the distribution of charge density in two different planes in figures 5 and 6. Figure 5 shows a sharing of charge between Ti and O due to Ti 3d and O 2p hybridization and figure 6 shows the nature of the bonding between Sr and TiO_3. The distribution of charge around the Sr site indicates that the bonding between Sr and

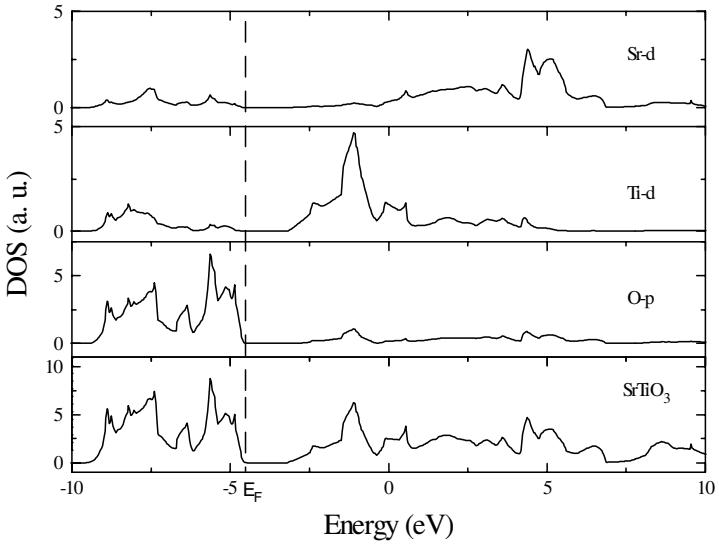

Figure 4. The angular-momentum- and site-projected densities of states of $SrTiO_3$. The dashed line shows the position of the Fermi level.

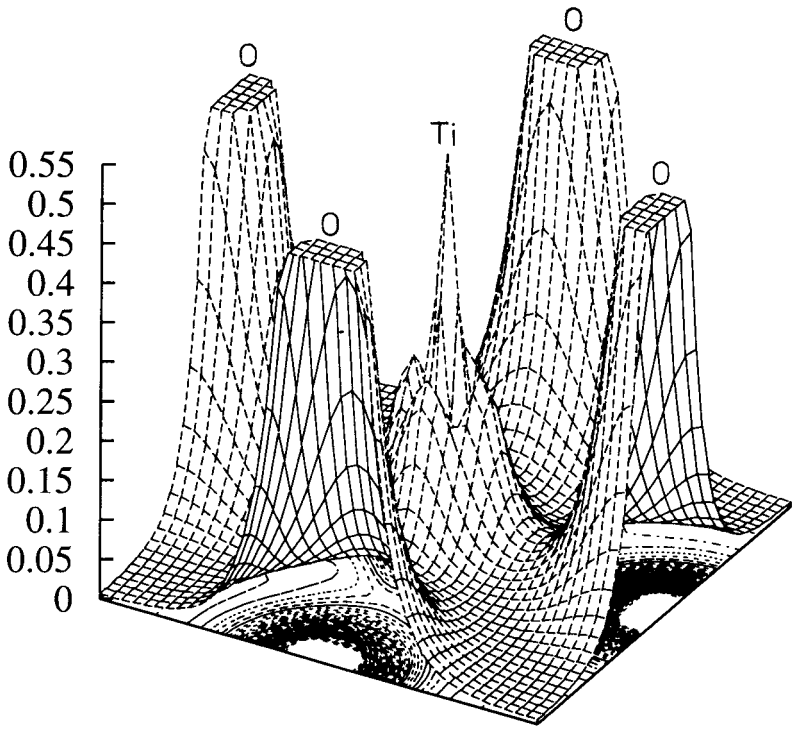

Figure 5. The valence charge-density contour in the (200) plane in three dimensions.

TiO_3 is mainly ionic. Further, the interatomic distance between the Ti and O is only 3.69 au and that between Sr and O is 5.22 au indicating that the bonding between Ti and O is covalent

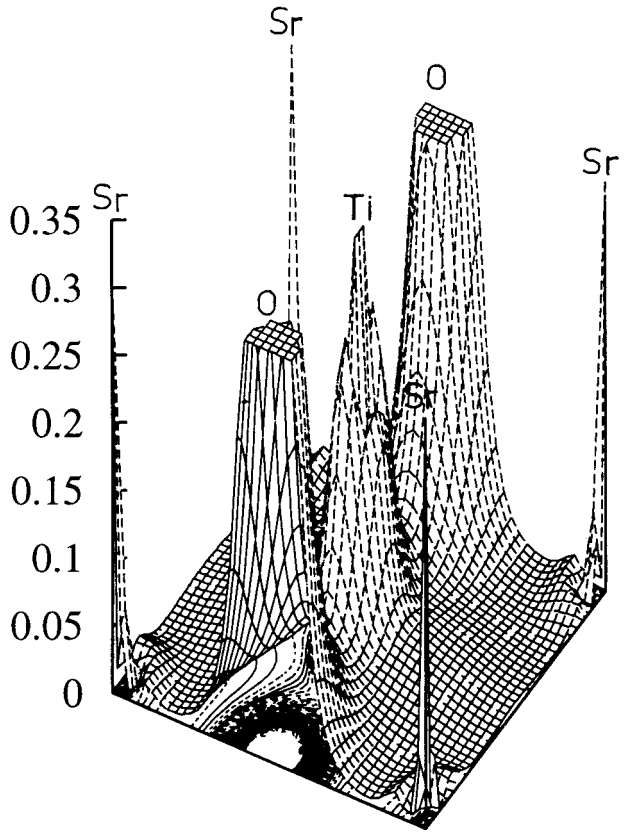

Figure 6. The valence charge-density contour in the (110) plane in three dimensions.

in nature. In support of this viewpoint, our calculated total valence charge in the Sr muffin-tin sphere is found to be 0.3 electrons. Further, the more electropositive nature of Sr compared with Ti and O confirms the presence of ionic bonding between Sr and TiO_3. The negligible charge density between Sr and TiO_3, as well as the very low electron population at the Sr site, much lower than that for the neutral Sr atom, is a clear indication of ionic bonding between Sr and TiO_3. Hence, the TiO_3 as a whole can be viewed as a negatively charged unit.

3.3. Optical properties

The interband optical functions calculated using expressions (2) and (3) are shown in figures 7 and 8. The imaginary part $\epsilon''(\omega)$ of the complex dielectric constant $\epsilon(\omega)$ shows mainly three peaks at 4.3, 5.6 and 6.3 eV. The first one is attributed to transitions from the O 2p (lower Γ_{15}) valence band to the Ti 3d ($\Gamma_{25'}$) conduction band (t_{2g}) and from the O 2p (upper Γ_{15}) valence band to the Ti 3d (Γ_{12}) conduction band (e_g). The second one is due to transitions from the O 2p (Γ_{25}) valence band to the Ti 3d (Γ_{12}) conduction band (e_g). The third peak originates from transitions from the O 2p (lower Γ_{15}) valence band to the Ti 3d (Γ_{12}) conduction band (e_g). These also explain the origin of the peak structure in the reflectivity ($R(\omega)$) and the absorption coefficient ($I(\omega)$) spectra.

The $\epsilon''(\omega)$ spectrum deduced from reflectivity measurements by Kramers–Krönig analysis is mainly composed of three peak structures. The first peak is located at around 5 eV, the second

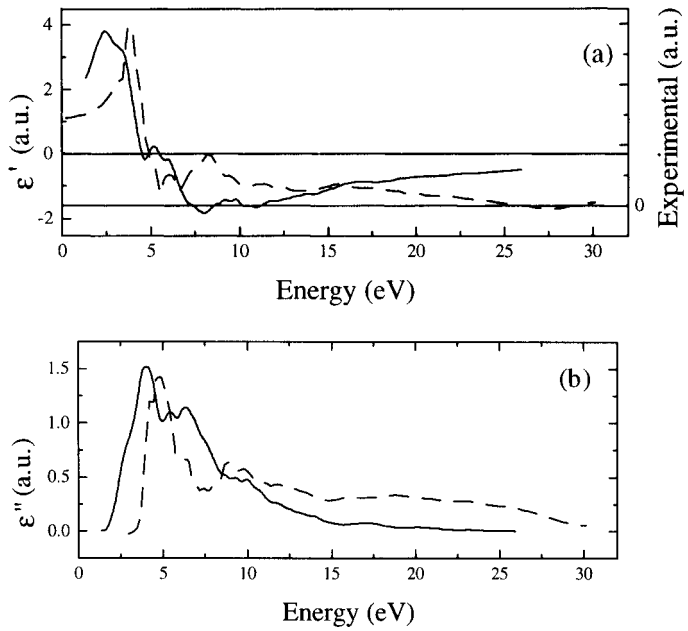

Figure 7. The calculated real ($\epsilon'(\omega)$) and imaginary ($\epsilon''(\omega)$) parts of the complex dielectric constant are compared with the experimental data [9]: dashed line: experimental; continuous line: theoretical.

one is at 6 eV and the third peak is located at around 9 eV. In figure 7 we have compared our calculated $\epsilon'(\omega)$ and $\epsilon''(\omega)$ spectra with experimental [9] data. The calculated values agree well as regards the three-peak structure in the $\epsilon''(\omega)$ curve with a slight (∼0.8 eV) shifting of the first and the second peaks from the experimental data. The calculated third peak is shifted by 2.3 eV from the experimental peak (figure 7). This discrepancy may be due to the inadequacy of the LDA as regards reproducing the band gap and the higher-energy excited states properly. Corrections like the 'scissors operator' technique correct these discrepancies somewhat. Absorption, energy-loss, refractive index and reflectivity measurements for $SrTiO_3$ crystals at room temperature in the cubic phase have been performed by several authors [8,9]. Figures 8(a), 8(b), 8(c), 8(d) and 8(e) show a comparison of calculated and experimental results for the reflectivity $R(\omega)$, absorption coefficient $I(\omega)$, refractive index $n(\omega)$, extinction coefficient $k(\omega)$ and energy loss $L(\omega)$. Overall, our theoretical spectra are found to be in good agreement with experiments for the lower-energy range. At higher energy the theoretical values do not follow the experimental trend. A possible reason for this departure is that we have not considered here the transition from the core to the conduction band which is expected above 14 eV. In the energy-loss spectrum $L(\omega)$ in figure 8(e), it is seen that the calculated peak appears at about 5 eV whereas the experimental peak appears at about 29 eV. It is to be noted that the condition of plasma resonance is fulfilled at the energy where $\epsilon'(\omega)$ crosses zero. So the discrepancy as regards the peak of $L(\omega)$ arises because our calculated $\epsilon'(\omega)$ becomes zero at around 5 eV as shown in figure 7(a) whereas the experimental $\epsilon'(\omega)$ becomes zero at around 27 eV. The effective number of valence electrons per unit cell contributing in the interband transitions can be calculated by means of the sum rule

$$n_{eff}(E_m) = \frac{2m}{Ne^2h^2}\int_0^{E_m} E\epsilon''(E)\,\mathrm{d}E$$

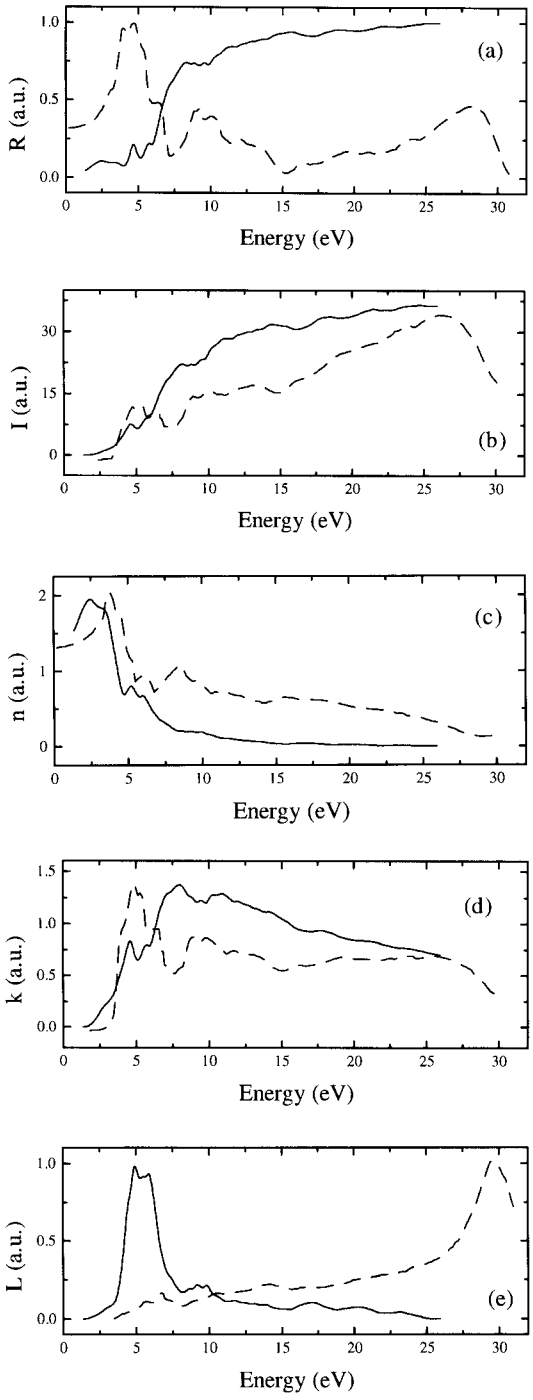

Figure 8. The calculated optical parameters are compared with the experimental results [9]: (a) the reflectivity spectrum $R(\omega)$, (b) the absorption coefficient $I(\omega)$, (c) the refractive index $n(\omega)$, (d) the extinction coefficient $k(\omega)$ and (e) the energy-loss spectrum $L(\omega)$; dashed line: experimental; continuous line: theoretical.

where E_m denotes the upper limit of integration. The quantities m and e are the electron mass and charge respectively. N stands for the electron density. The results are shown in figure 9. $n_{eff}(E_m)$ reaches a saturation value above 20 eV. This shows that the deep-lying valence orbitals do not participate in the interband transition.

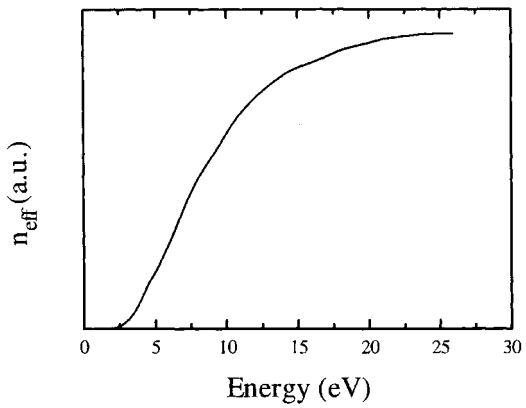

Figure 9. The calculated effective numbers of electrons (n_{eff}) participating in the interband optical transitions.

4. Conclusions

We have made a detailed investigation of the electronic structure and optical properties of paraelectric $SrTiO_3$ in the cubic phase using the TB-LMTO method. The calculations show that the fundamental gap of $SrTiO_3$ is direct at the gamma point. Our calculated fundamental gap $\sim$1.4 eV is smaller than the experimentally reported value 3.3 eV, as it should be because of the discontinuity in the exchange–correlation potential, which is not taken into account. Using the site- and angular-momentum-projected DOS and band structure we have analysed the interband contribution to the optical properties. The chemical bonding of $SrTiO_3$ is also analysed. The TiO_3 complex is bonded mainly by covalent bonds and the Sr and TiO_3 constituents are bonded ionically. The total DOS obtained from our first-principles calculations are compared with experimental results [6]. We have examined the energy-dependent dielectric constants as well as related quantities such as reflectivities, absorption coefficients, energy-loss functions, refractive indices and extinction coefficients, and compared with the experimental results at room temperature for $SrTiO_3$ in the cubic phase. Lastly, the effective numbers of electrons per unit cell participating in the interband transitions are calculated.

References

[1] Lines M E and Glass A M 1977 *Principles and Applications of Ferroelectrics and Related Materials* (Oxford: Clarendon)
[2] Müller K A and Burkard H 1979 *Phys. Rev.* B **19** 3593
[3] Zhong W and Vanderbilt D 1996 *Phys. Rev.* B **53** 5047
[4] Lytle F W 1964 *J. Appl. Phys.* **35** 2212
[5] Spitzer W G, Miller R C, Kleinman D A and Howarth L E 1962 *Phys. Rev.* **126** 1710
[6] Perkins P G and Winter D M 1983 *J. Phys. C: Solid State Phys.* **16** 3481
[7] Viana R, Lunkenheimer P, Hemberger J, Böhmer R and Loidl A 1994 *Phys. Rev.* B **50** 601
[8] Cardona M 1965 *Phys. Rev.* **140** A651

[9] Bauerle D, Braun W, Saile V, Sprussel G and Koch E E 1978 *Z. Phys.* B **29** 179
[10] Nes O M, Müller K A, Suzuki T and Fossheim F 1992 *Europhys. Lett.* **19** 397
[11] Perry C H, Khanna B N and Rupprecht G 1964 *Phys. Rev.* **135** A408
[12] Servoin J L, Lupsin Y and Gervais F 1980 *Phys. Rev.* B **22** 5501
[13] Müller K A, Berlinger W and Tosatti E 1991 *Z. Phys.* B **48** 277
[14] Jauch W and Palmer A 1999 *Phys. Rev.* B **60** 2961
[15] Fleury P A, Scott J F and Worlock J M 1968 *Phys. Rev. Lett.* **21** 16
[16] Shirane G and Yamada Y 1969 *Phys. Rev.* **177** 858
[17] Anderson O K and Jepsen O 1984 *Phys. Rev. Lett.* **53** 2571
[18] Cohen R E and Krakauer H 1990 *Phys. Rev.* B **42** 6416
[19] Cohen R E 1992 *Nature* **358** 136
[20] Cohen R E and Krakauer H 1992 *Ferroelectrics* **136** 65
[21] Singh D J and Boyer L L 1992 *Ferroelectrics* **136** 95
[22] King-Smith R D and Vanderbilt D 1994 *Phys. Rev.* B **49** 5828
[23] King-Smith R D and Vanderbilt D 1992 *Ferroelectrics* **136** 85
[24] Wyckoff R W G 1964 *Crystal Structures* 2nd edn, vol 2 (New York: Chemical Catalog Company Incorporated)
[25] Ravindran P, Delin A, Johansson B and Eriksson O 1999 *Phys. Rev.* B **59** 1776